# Probing the interface and individual layers in cuprate/manganite heterostructures by Raman Spectroscopy

F. Lyzwa,[1, 2, 3] A. Chan,[1, 4] K. Fürsich,[5] B. Keimer,[5] C. Faugeras,[6] Yu. G. Pashkevich,[3, 7] C. Bernhard,[3] M. Minola,[5] and B.P.P. Mallett[8, 4]

[1] *Department of Physics and School of Chemical Sciences, The Photon Factory, The University of Auckland, 38 Princes Street, Auckland, New Zealand*
[2] *National Synchrotron Light Source II, Brookhaven National Laboratory, Upton, New York, USA*
[3] *Department of Physics and Fribourg Center for Nanomaterials, University of Fribourg, Chemin du Musée 3, CH-1700 Fribourg, Switzerland*
[4] *The MacDiarmid Institute for Advanced Materials and Nanotechnology and The Dodd Walls Centre for Quantum and Photonic Technologies, New Zealand*
[5] *Max-Planck-Institut für Festkörperforschung, Heisenbergstrasse 1, 70569 Stuttgart, Germany*
[6] *LNCMI, UPR 3228, CNRS, EMFL, Université Grenoble Alpes, 38000 Grenoble, France*
[7] *O. Galkin Donetsk Institute for Physics and Engineering NAS of Ukraine, UA-03028 Kyiv, Ukraine*
[8] *Robinson Research Institute, Victoria University of Wellington, 69 Gracefield Road, Lower Hutt 5010, New Zealand*

(Dated: 17 April 2024)

We report a comprehensive set of polarized Raman spectra on thin-film multilayers of the high-$T_c$ superconductor $YBa_2Cu_3O_7$ and electrically insulating manganites $R$MnO$_3$ ($R =$ rare-earth partially substituted with Group II elements) hosting magnetic, charge and orbital order (COO). Such multilayers have been shown to exhibit a unique insulating-to-superconducting transition that is induced by magnetic field, electric field or by tailoring the chemical composition of the $R$-site of the manganite. The Raman spectra show significant Jahn-Teller distortions of the manganite structure, which correlate with COO, approximately 90 K above the magnetic ordering temperature of 140 K. Based on the Raman data and earlier electrical transport studies of single-layer manganite films, we argue that the manganite layers in our heterostructures remain electrically insulating across the range of temperatures, dopings and magnetic fields investigated. The Raman spectra show a pronounced red-shift and broadening of lattice vibrations around 200 cm$^{-1}$ in the multilayers compared to those of manganite films may indicate hybridization with $YBa_2Cu_3O_7$ phonons. We also observe additional excitations at 690 cm$^{-1}$ and 830 cm$^{-1}$ that are absent in the single films or bulk responses, which we discuss to originate from the cuprate/manganite interface. These observations demonstrate that the phonon spectrum is significantly modified in our multilayer samples. This is expected to play an important role in the mechanism of the insulating-to-superconducting transition found in these cuprate-manganite multilayers.

**keywords:** $YBa_2Cu_3O_7$, charge and orbital ordering, superconductivity, manganite, thin film heterostructures, Raman spectroscopy, interfaces, hybridization

## I. INTRODUCTION

Thin-film multilayers comprising metal-oxides host a wide range of emergent, tunable and potentially useful characteristics[1–9], which result from interactions across the interface such as spin and orbital reconstruction, charge transfer and phonon-coupling[3–6,10] as well as some as-yet unidentified mechanisms[11,12]. A showpiece are multilayers of the cuprate high-temperature superconductors (high-$T_c$ SC) and rare-earth manganites, exhibiting a range of emergent properties, such as modified spin-states at the interface and long-range electron-phonon coupling transfer[8]. These heterostructures are a powerful platform to study the interplay between magnetic and superconducting order[13?] and the charge- and orbital ordering (COO)[14]. They allow for extended functionality such as super-spin valves[15], and could be incorporated in future electronic devices[16].

Furthermore, they provide a novel route to understanding high-$T_c$ SC in the cuprates by way of the response of the superconducting condensate to the electronic and magnetic state of the manganite.

Raman spectroscopy has been widely used to measure the optical response of $YBa_2Cu_3O_{7-\delta}$ (YBCO) and manganite single crystals to study phonons (and phonon anomalies) and their potential coupling to superconductivity and other electronic states[17–19], charge ordering[20–24], electronic scattering associated with superconductivity[18,25] as well as scattering related to magnetic excitations[26,27] through to proximity-induced superconductivity[28]. The number, energy and linewidth of phonons in the Raman spectra indicate a particular space-group symmetry and crystalline quality.

Measuring the Raman response of thin films, and especially multilayers and superlattices with a large number of interfaces, is more complex. Using Macro-Raman Scattering is unsuitable to study these systems, because of a normally very strong and thus dominating response from the substrate compared to the one of thin films with thicknesses in the nanometer range. A solution to this issue is to use confocal Raman spectroscopy, where the film's response can be isolated. This approach revealed a transfer of the electron-phonon coupling strength between superlattice layers[6], spin and charge ordering in nickelate superlattices[29] and the COO in some cuprate/manganite heterostructures[12,30], and ferroelastic Jahn-Teller domains in $LaMnO_3$ thin films[31]. However, the majority of previous studies focused on a limited range of manganite compositions and periodicity configurations, which limits the possibility to make comprehensive conclusions on the role of the interface and of single layers.

Here, we detail the Raman response of high-quality thin-film multilayers of manganites $R\mathrm{MnO}_3$ and the superconductor YBCO, which have been shown to host a highly unusual superconducting ground state that is electrically insulating on a macroscopic scale[11]. Our main interest in this study is to investigate the emerging phenomena observed in the heterostructures that arise from the interface and which cannot be attributed to the bulk response. $R$ is chosen so as to alter the electronic and magnetic properties of the manganite[30], which in turn induces the putative granular-superconducting state of the YBCO that leads to an insulating macroscopic response. Our wider aim is to characterize the salient properties of the manganite which induce these unusual superconduting states, including magnetic, charge, and orbital ordering of the manganite. Whilst Raman spectroscopy is an indirect probe of such states, it is instructive as it is complementary to bulk probes. For example, the electrical transport properties of the manganite can be difficult to ascertain from direct electrical transport measurements on multilayer films containing the highly conducting YBCO. By studying the effects of magnetic field, temperature, scattering polarization and sample composition, and in comparison to literature pertaining to bulk single crystals, we confirm the optimal doping of the YBCO and insulating state of manganite in multilayer compositions that exhibit the insulator-to-superconducting transition. We further report on two novel Raman-active modes at 690 $\mathrm{cm}^{-1}$ (86 meV) and 830 $\mathrm{cm}^{-1}$ (103 meV), and show a potential hybridization of cuprate and manganite phonon modes in the multilayers.

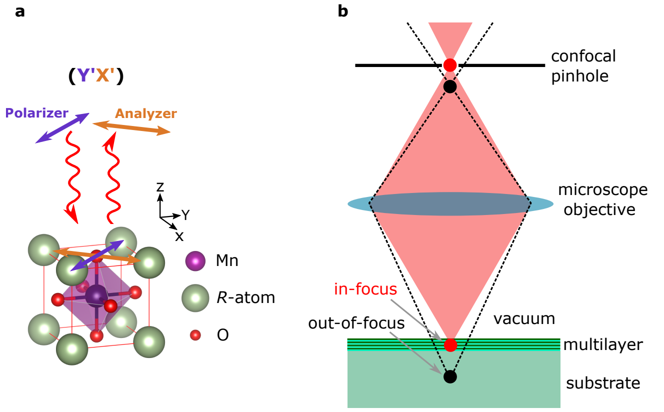

FIG. 1. Principle of polarized confocal Raman spectroscopy. (a) Sketch of the incident (violet) and scattered (orange) light polarization on a $R\mathrm{MnO}_3$ unit cell. As an example, an $z(X'Y')\bar{z}$ - configuration after Porto's notation, is shown. (b) The laser light is focused onto the sample surface, so that scattered light contributions from out-of-focus points (such as from the substrate) are suppressed by the confocal pinhole[33].

## II. MATERIALS AND METHODS

### A. Materials

Epitaxial thin films of the cuprate superconductor $YBa_2Cu_3O_7$(YBCO) and perovskite-phase manganite $R\mathrm{MnO}_3$, with $R$ = $Pr_{0.5}La_{0.2}Ca_{0.3}$ (PLCMO), $La_{1-x}Ca_x$ (LCMO) or $Nd_{1-x}(Ca_{1-y}Sr_y)_x$ (NCSMO), are grown on $La_{0.3}Sr_{0.7}Al_{0.65}Ta_{0.35}O_3$ (LSAT) substrates that are (001)-oriented (from Crystec) by pulsed laser deposition (PLD) using an excimer KrF laser ($\lambda = 248$ nm) and following the detailed growth and characterization process described in Refs.[12,32]. The films' thicknesses range from 1 to 100 nm and are capped by a 1-2 nm thin layer of $LaAlO_3$ to protect the surface of the manganite or cuprate top film. In this manner, the layer thicknesses show bulk-like responses. Ideally, one would make a thickness-dependent study, however, thinner layers would lead to proximity effects and larger total sample thicknesses would decreas film quality. The superlattice samples here presented have a periodicity of 10 bilayers (Cu/Mn). The samples have a small interface roughness ($\sim$ 0.5 nm) and minimal chemical diffusion across the interface; this has been determined by e.g. x-ray reflectivity experiments, with representative quality characterization results found in the supplementary materials of Refs. 11 and 12. Single layers were synthesized for the purpose of being the reference samples. The effect of the Cu/Mn interface was investigated by obtaining the Raman response of trilayers with manganite-cuprate-manganite configuration. This response we expected to be enhanced in superlattice samples comprising multiple repetitions of a manganite-cuprate bilayer block, with the first and the last film layer (excluding the $LaAlO_3$ capping film) being the manganite.

### B. Methods

The zero-field Raman spectroscopy experiments were carried out using the 632.8 nm excitation line of a HeNe laser and recorded on a commercial HORIBA LabRAM HR800 spectrometer. The measurements reported in the manuscript were performed in full back-scattering geometry expressed in Porto's notation. As sketched in Fig. 1a, $z(X'Y')\bar{z}$ indicates back-scattering with incident polarization 45° to the Mn-O nearest-neighbour bond with the cross-polarized scattered light measured. The spectral resolution of approximately 1 $\mathrm{cm}^{-1}$ is set by the 600 lines/mm grating, and the spatial resolution in the horizontal (vertical) direction of about 10 μm (a few micrometers) is defined by the optical components. The laser was focused with a ×100 long-working distance objective lens with a short depth of focus, NA= 0.6, which was positioned with an accuracy of 0.5 μm such that the focus is centered on the film[29,34]. In addition, a 50 μm confocal hole is placed along the scattered light path to minimize the Raman responses from out-of-focus points, such as the substrate contribution (see Fig. 1b). Collection times for each spectrum were typically 30 min. The residual substrate contribution was subtracted from the spectra using reference measurements for which the beam focus was moved into the substrate:

$$I_{\mathrm{raw}} = \left(I_{z=0} - f_{\mathrm{ss}} I_{\mathrm{ss}}\right) / \left(1 - f_{\mathrm{ss}} - f_{\mathrm{vac}}\right) \tag{1}$$

Here, $I_{z=0}$ is the spectrum measured at the optimal focal height for the film, $f_{\mathrm{ss}}$ is a fitting parameter that represents the fraction of the focal volume which still probes the substrate at $z = 0$ and $I_{\mathrm{ss}}$ is the substrate spectrum obtained by moving the focus 30 µm below the film surface ($z = 30\,\mu\mathrm{m}$). $f_{\mathrm{vac}}$ is an additional fitting parameter representing the fraction of the focal volume above the surface of the film when $z = 0$, which does not contribute to the Raman response. It adjusts the magnitude of $I_{\mathrm{raw}}$ and may be used to normalize the spectra. Unless explicitly mentioned otherwise, we set $f_{\mathrm{vac}} = 0$ in this work.

Two volume Bragg-grating filters in combination with an Ultra Low Frequency Filter allowed us to efficiently reject Rayleigh-scattering, facilitating data collection down to 4.5 $\mathrm{cm}^{-1}$ on either side of the elastic scattering from the laser.

The sample temperature was controlled by means of a He flow cryostat and laser heating effects were minimized by keeping the laser power below 1 mW. All reported Raman spectra in the manuscript are corrected for the Bose thermal factors. For Stokes scattering

$$R(\nu) \cong I_{\mathrm{raw}} \left[1 - \exp\left(\frac{-\hbar\nu}{k_{\mathrm{B}} T}\right)\right] \tag{2}$$

where $T$ is the temperature and $R(\nu)$ is the imaginary part of the Raman susceptibility[35,36].

Raman-active excitations observed in the spectra were fitted using pseudo-Voigt line shapes

$$I(\nu) = SW\left[\eta L(\nu, \nu_0, \gamma) + (1 - \eta)\, G(\nu, \nu_0, \Delta)\right] \tag{3}$$

which convolute the instrumental resolution with the intrinsic line-width of the Raman mode. In this expression $L(\nu, \nu_0, \gamma) = \gamma^2 \pi^{-1} \left[\gamma^2 + (\nu - \nu_0)^2\right]^{-1}$ is a Lorentzian line shape, $G(\nu, \nu_0, \Delta) = \left(\sqrt{\pi}\Delta \ln 2\right)^{-1} \exp\left[-\ln 2.(\nu - \nu_0)^2 \Delta^{-2}\right]$ a Gaussian line shape and $\eta$ a mixing parameter used to approximate the exact convolution function[37]. $SW$ is the area under the curve, $\nu_0$ the peak-center and $\gamma$ the half-width at half-maximum (HWHM) of the mode.

The magnetic-field-dependent Raman scattering experiments were performed from zero to 13 Tesla. The data was taken at $T = 5$ K after zero-field cooling and under excitation of a 515.1 nm laser light beam in quasi-$z(XX)\bar{z}$ scattering geometry. In this experiment, it was necessary to tilt the sample 30° away from true back-scattering geometry to suppress the Rayleigh scattering. This also results in the applied magnetic field direction being at a 30 degree offset from the film normal (30 degrees off the $c$-axis of the YBCO). The analysis is in analogy to the zero-field spectra, which will be further discussed in the respective Results section.

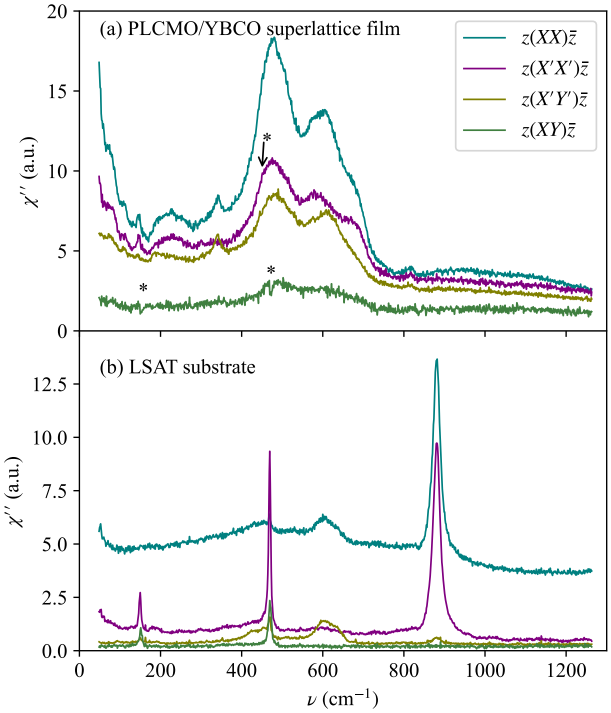

FIG. 2. Polarization dependence and isolation of the pure thin film response. The spectra demonstrate the four accessible polarisation configurations for (a) a PLCMO(10 nm) / YBCO(7 nm) superlattice sample (after the substrate correction) with ten bilayer repetitions and a total film thickness of 180 nm at 10 K, and (b) an LSAT (001) substrate. The black asterisks in (a) show artefacts which result from a residual substrate contribution after correction.

## III. RESULTS

### A. Exemplar: $\mathrm{Pr}_{0.5}\mathrm{La}_{0.2}\mathrm{Ca}_{0.3}\mathrm{MnO}_3$ / $\mathrm{YBa}_2\mathrm{Cu}_3\mathrm{O}_7$ multilayers

We start by presenting Raman scattering spectra demonstrating the overall spectral features resolved from our thin-film multilayers. Figure 2(a) shows the spectra taken at 10 K for a PLCMO(10 nm) / YBCO(7 nm) superlattice with ten bilayer repetitions and a total film thickness of 180 nm (see Materials section for details) for all four unique and accessible polarization configurations for our experimental set up.

The spectra of an LSAT single crystal, which served as a substrate for the thin films studied in this work, are taken at a temperature of 10 K and are shown in Figure 2(b). From 10 to 300 K the spectra of LSAT do not change significantly, which is expected since there is not any known structural or electronic phase transitions in this temperature range in this material, with the symmetry being conserved. Previously reported spectra taken at room temperature are in good agreement[38,39]. In most cases, the substrate contribution to the raw spectra can be unambiguously and effectively subtracted by the procedure described in the Methods section. There are however a few spectral regions where, for some polarization configurations, the substrate subtraction procedure leads to artefacts in the spectra (marked by black asterisks in Figure 2(a)).

The spectra of a cuprate-manganite multilayer thin film in Figure 2(a) reveal multiple and overlapping peaks and a non-zero 'background' intensity. Except for additional back-folded $c$-axis phonon modes[40] at around $\nu \approx 10\,\mathrm{cm}^{-1}$, the presented spectral range shows all the features that we observed. That is, we do not see additional spectral features out to $4000\,\mathrm{cm}^{-1}$ such as might be expected for two-magnon scattering from the YBCO[41], or spurious fluorescence or spectral features associated with adsorbed ice[42].

When comparing the response under the various polarization configurations, it is clear that spectral features in the $z(XY)\bar{z}$ configuration are weak. This polarization configuration also exhibits a relatively weak Raman response in single crystals of $\mathrm{YBa_2Cu_3O_7}$[43] and comparable manganites[23] from which we infer that our multilayer films maintain throughout a good alignment of the in-plane crystallographic axes. We note that those in-plane crystallographic axes are finely twinned in our films, so that any orthorhombic distortion of the crystal structure in our films does not lead to a measurable difference under 90 degrees in-plane rotation of the sample. The most intense Raman response is observed for the $z(XX)\bar{z}$ configuration, which again compares well with expectations from previous measurements on single crystals[17,23,43]. This configuration however shows a convolution of spectral features that can be observed in the $z(X'X')\bar{z}$ and $z(X'Y')\bar{z}$ configurations, as expected from symmetry arguments applied to the single crystals[43]. As such, our measurements have focused on these latter two polarization configurations. For $\mathrm{YBa_2Cu_3O_6}$, having a tetragonal crystal structure with point-group $D_{4h}$, $z(X'X')\bar{z}$ selects modes of $A_{1g}+B_{2g}$ symmetry and $z(X'Y')\bar{z}$ selects for $B_{1g}$.

To better understand the origin of the various features in the Raman spectra of our films, we show in Figure 3 (a,b) the spectra taken at 10 K from (i) a 100 nm film of the bare manganite PLCMO, (ii) a cuprate/manganite trilayer, PLCMO(20 nm) / YBCO(7 nm) / PLCMO(20 nm) and (iii) the PLCMO(10 nm) / YBCO(7 nm) superlattice from Figure 2(a). The figure further contains literature data from single crystals of YBCO[18,20] and a manganite with a somewhat similar electronic and magnetic ground state, $\mathrm{La_{0.5}Ca_{0.5}MnO_3}$[2345]. Panel (a) of the Figure shows $z(X'X')\bar{z}$ and panel (b) shows $z(X'Y')\bar{z}$ scattering.

Based on these comparative observations we can assign contributions to the spectra as deriving from either the manganite, YBCO, or as unique to the multilayer films. The spectra were fitted using a number of pseudo-Voigt lines and a quadratic-background, as described in the Methods. An example of the fitting using the trilayer data from Figure 3 is shown in Figure 4. This spectral decomposition, and corresponding summary of peak energies in Table I, highlights how the majority of the components are already present in the bare manganite (green peaks), with only a few features from the $\mathrm{YBa_2Cu_3O_7}$ (purple peaks) visible. Some components have been labeled as 'multilayer' (orange peaks) since they only appear in our multilayer film spectra. A pronounced increase in the response at low-wavenumber was determined to be a background, and was fitted with a quadratic function (grey line).

We now examine in more detail the relation of these various spectral components with the structural and electronic properties of the films.

## B. Response from the $\mathrm{YBa_2Cu_3O_7}$

The cuprate superconductor YBCO has five main Raman active phonon modes for our off-resonant laser energy of 1.96 eV[25]. These are observed at approximately 120, 150, 340, 430 and $500\,\mathrm{cm}^{-1}$. The latter two modes involve predominantly oxygen vibrations and are masked by the much stronger manganite modes. The $120\,\mathrm{cm}^{-1}$ mode involves predominantly the $c$-axis motion of the Ba ions. Its intensity is enhanced by the onset of superconducting correlations[46–48] and its frequency softens by several wavenumbers[17]. We can observe this mode in our data as a weak spectral feature, but only for the superlattice samples. Motion of the Cu ions along the $c$-axis leads to the $150\,\mathrm{cm}^{-1}$ mode, which however overlaps with a manganite mode at the same frequency. It may be possible to enhance the response of this mode using a laser light wavelength greater than the 632.8 nm used here[48], although it was not investigated in this work.

The most prominent feature from the YBCO in our thin-film spectra is the peak at $340\,\mathrm{cm}^{-1}$ seen in the $z(X'Y')\bar{z}$ polarization channel. This phonon mode arises from an anti-phase $c$-axis motion of the $\mathrm{CuO_2}$ layer oxygens and is well known to be strongly renormalized across the superconducting transition for optimally and over doped YBCO[17]. Here, the mode is observed as a weak peak in the trilayer samples with a half-width at half-maximum of $10\,\mathrm{cm}^{-1}$, consistent with that obtained for single crystals of YBCO[17,20]. The phonon is however much clearer in the superlattice samples, since there is approximately ten times the volume of YBCO probed by the laser. With the better signal-to-noise for this mode in the superlattice samples, we reliably detect a broadening of the phonon mode of about $2\,\mathrm{cm}^{-1}$ (15%) at temperatures below $T_\mathrm{c} \approx 70\,\mathrm{K}$. The broadening is a result of electron-phonon coupling between this phonon mode and itinerant quasi-particles[25]. The amount of broadening we observe below $T_\mathrm{c}$ is consistent with that expected for optimally doped and overdoped (i.e. with hole doping levels higher than $p \approx 0.14$) rather than underdoped YBCO[17]. In addition, it is observed in single-crystals that this mode exhibits a clear asymmetry due to the electron-phonon interaction[25], with its line shape well-described by a Fano resonance. The superlattice spectra are consistent with the development of such an asymmetrical line shape below $T_\mathrm{c}$.

From these observations we conclude that the YBCO in these multilayer films is near optimally doped and with crystalline quality comparable to single crystals. The quasi-particle states of the YBCO near the Fermi energy are renormalized below $T_\mathrm{c}$.

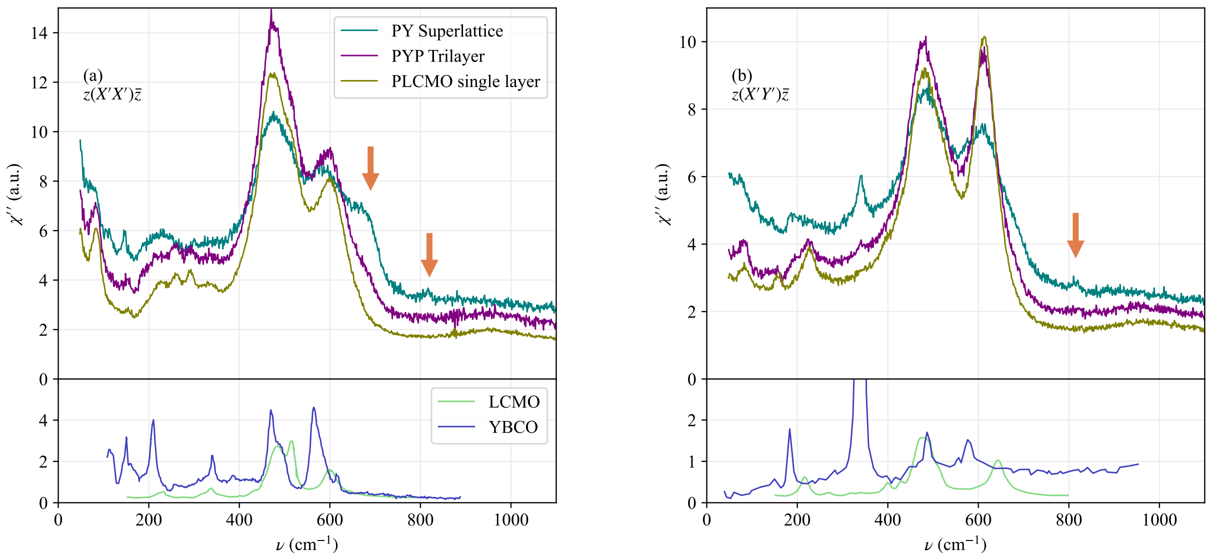

FIG. 3. Raman spectra taken at 10 K for a 100 nm single layer PLCMO manganite film, a PLCMO(20 nm) / YBCO(7 nm) / PLCMO(20 nm) (PYP) trilayer and PLCMO(10 nm) / YBCO(7 nm) (PY) superlattice with $z(X'X')\bar{z}$ in panel (a) and $z(X'Y')\bar{z}$ in panel (b). By way of comparison, the sub-panels show the data taken on single crystals of $La_{0.5}Ca_{0.5}MnO_3$[23] and $YBa_2Cu_3O_{6.95}$[20,44]. The orange-colored arrows indicate the peaks being unique to the multilayer samples.

| Polarizer configuration | Symmetry | Manganite [cm$^{-1}$] | $YBa_2Cu_3O_7$ [cm$^{-1}$] | Multilayer [cm$^{-1}$] |
|---|---|---|---|---|
| $z(X'Y')\bar{z} = z(Y'X')\bar{z}$ | $B_{1g}$ | 84, 192, 226, *280*, 480, 532, 613, *1000* | 340 | 190, 830 |
| $z(X'X')\bar{z} = z(Y'Y')\bar{z}$ | $A_{1g} + B_{2g}$ | 84, 153, 221, 260, *280*, 292, 335, 470, 518, 601, *1000* | 120 | 192, 690, 830 |

TABLE I. Peak positions as observed for the two polarizer configurations $z(X'X')\bar{z}$ and $z(X'Y')\bar{z}$, with the column labelled 'Symmetry' indicating the corresponding excitation symmetry for the $YBa_2Cu_3O_6$ point group case, $D_{4h}$. The peaks are grouped according to whether they are observed in the spectra of the single-layer manganite films or only in the YBCO-manganite multilayer films, or ascribed to the bulk $YBa_2Cu_3O_7$ response. Italicized modes in the manganite column indicate particularly broad spectral features. Note that not all modes of the manganite and $YBa_2Cu_3O_7$ are listed here, only those that are needed to fit our data.

### C. Response from the manganite

The majority of peaks in the multilayer spectra derive from the manganite layer, as can readily be seen from Figures 3 and 4. The manganites studied here adopt a perovskite crystal structure. An ideal cubic perovskite structure has no Raman-active phonon modes, which shows that the symmetry of our manganite has been lowered due to a combination of distortion of the oxygen octahedra (e.g. a Jahn-Teller distortion), A-site ions off-centered and/or octahedral tilting[49,50]. Manganites exhibiting magnetic, charge and orbital ordering (as we argue to be the case in our samples) adopt a particularly low symmetry where the monoclinic crystallographic space group $P2_1/m$ is used to describe diffraction patterns from similar, bulk manganites. Group-theory analysis shows 54 allowed first-order Raman-active phonon modes for this space group. Abrashev *et al.*[23] were however able to analyze their data from a charge-ordered manganite in terms of the simplified orthorhombic space group, *Pmma*, which does not include $MnO_6$ octahedral tilts. In this case the number of allowed Raman-active modes is reduced to 21 in total, and for the $z(X'X')\bar{z}$ and $z(X'Y')\bar{z}$ sample scattering configurations that we focus on there are 7 $A_g$ and 7 $B_{2g}$ modes expected, respectively.[51]

Figures 2 and 3 show however that are at least 9 first-order peaks in $z(X'X')\bar{z}$ and 6 in $z(X'Y')\bar{z}$, with additional weaker or overlapped peaks possible. This simple counting exercise implies that quasi-static tilting of the $MnO_6$ octahedra in our films is significant enough to lead to at least two additional ($A_g$) Raman modes observed in the $z(X'X')\bar{z}$ configuration.

In this work, our primary interest in the observed spectral features are the implications regarding the structural and electronic properties of the films. Although it is not straightforward to unambiguously assign all the observed spectral features to specific modes/excitations[21,23], insight relating the Raman response to magnetic, structural and electronic properties of bulk manganites has been accumulated in the literature through studies that vary composition, polarization configuration, temperature and magnetic field in combination with theoretical analysis. Here, we draw on these results and this

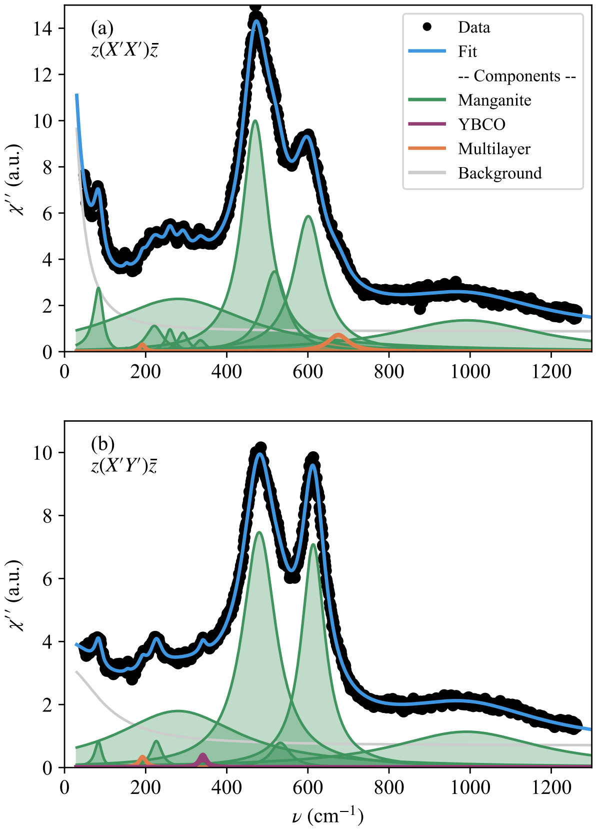

FIG. 4. Spectral decomposition of the Raman response for a PLCMO(20 nm) / YBCO(7 nm) / PLCMO(20 nm) (PYP) trilayer at 10 K, in (a) $z(X'X')\bar{z}$ and (b) $z(X'Y')\bar{z}$ scattering geometry.

approach to investigate the properties of the manganite as thin films and in multilayer thin films.

In Figure 5 we present data that highlight the manganite response at 10 K for a range of thin-film compositions, $R$MnO$_3$; $R$ = Pr$_{0.5}$La$_{0.2}$Ca$_{0.3}$ (PLCMO 100 nm), Nd$_{1-x}$(Ca$_{1-y}$Sr$_y$)$_x$ (NCSMO) with $x = 0.35$ and $y = 0.3$ and a trilayer of NCSMO with $x = 0.5$, $y = 0.5$ and YBCO. Above 800 cm$^{-1}$ the spectra lie on top of each other, but in Figure 5 they are offset as indicated by the zero-intensity lines at the left hand side in the panels. The various $R$ (i.e. rare-earths and alkali earth metal compositions) were chosen to tune the amplitude of COO and its coherence[30,52]. This is illustrated in Fig. 5(c) where we sketch a phase-diagram for the manganite electronic and magnetic ground state and an indicative placement of our thin-film samples in this phase space (noting that the phase diagram was derived from measurements on bulk samples and may not accurately represent the ground state of our thin-film samples). Several phonon modes are related to the magnetic, metallic and/or charge-and-orbital order and are of particular focus here.

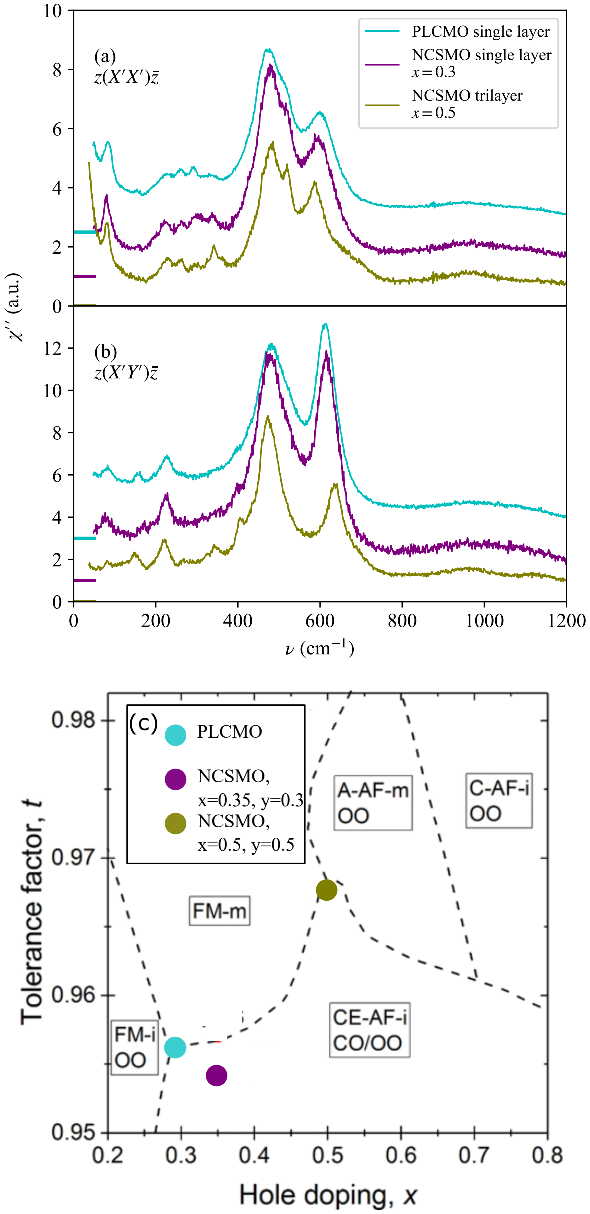

FIG. 5. Variation of $R$-site atom. The spectra were taken at 10 K and compare the response between a PLCMO and NCSMO thin film at $x = 0.3$ doping and a NYN multilayer at $x = 0.5$ doping of the NCSMO. Panel (a) shows $z(X'X')\bar{z}$ scattering geometry and panel (b) $z(X'Y')\bar{z}$. (c) A ground-state phase diagram for bulk manganites adapted from Ref.[52] with approximate location of our samples indicated.

We start with the NCSMO $x = 0.35$, $y = 0.3$ and PLCMO spectra, where YBCO-manganite multilayers with these manganite compositions have exhibited a magnetic-field and electric-field induced coherence of the superconducting state. In most aspects, the Raman spectra of such films are identical. This is not surprising, as $x$ and $y$ for the NCSMO film were chosen to give similar lattice parameters and bond-angles (as characterized by the tolerance factor) to the PLCMO film. There are some minor differences with regard to the peak positions and widths, discussed below, however the similarity of the Raman spectra demonstrates that this strategy was successful. The two manganite materials have similar structural properties when grown as films, and given the coupling between lattice charge and magnetic degrees of freedom in the manganites suggests similar electronic and magnetic properties are shared between the manganite compositions in $\sim 100$ nm films. We now discuss this last point in more detail.

The vibrational mode seen at approximately $230\,\mathrm{cm}^{-1}$ in $z(X'Y')\bar{z}$ involves a rotation of the $MnO_6$ octahedra[53]. The intensity of the mode in Raman spectra was observed to increase markedly below the ferromagnetic magnetic phase transition in $La_{0.7}Ca_{0.3}MnO_3$, in addition to a marked hardening[6,54]. However, in our earlier Raman studies of YBCO-NCSMO thin film multilayers, this mode was detected at temperatures above the magnetic ordering temperature as observed by magnetization measurements, but in line with the onset of COO[12,30]. For our PLCMO films the mode is centered at $225\,\mathrm{cm}^{-1}$, and its HWHM at 10 K is about $20\,\mathrm{cm}^{-1}$.

The phonon mode seen at approximately $470\,\mathrm{cm}^{-1}$ in $z(X'Y')\bar{z}$ is allowed in the presence of a (static or dynamic) Jahn-Teller distortion and involves bending the O of the $MnO_6$ octahedra. The strength of these modes, presented by the peak area *SW*, is related to the degree of Jahn-Teller distortion.

The vibration lifetime, $\tau = 1/\gamma$, which in our case is $\sim 10^{-14}$ s, has been related to the time between two consecutive hops of any doped charge-carrier on the Mn (e.g. the mean lifetime of a $Mn^{3+}$ before a hole hops onto that site to convert into a $Mn^{4+}$)[24,55]. This is in turn related to the metallicity of the manganite, with the hole-hopping rate becoming faster than the Jahn-Teller mode vibration in the metallic state leading to a low intensity for this mode and the $610\,\mathrm{cm}^{-1}$ mode[24]. The reverse situation sees a static Jahn-Teller distortion of the $Mn^{3+}$ $MnO_6$ octahedra, which can order with the $Mn^{4+}$ octahedra to form the COO insulating state. Magnetic-field and compositional studies by Tomioka *et al.*[21] confirmed that the $470\,\mathrm{cm}^{-1}$ mode and the $610\,\mathrm{cm}^{-1}$ mode (which is a breathing type mode involving the O of the $MnO_6$ octahedra[22,23] and the central Mn) are signatures of COO.

We find that the *SW* of the $470\,\mathrm{cm}^{-1}$ mode is about eight times that of the $230\,\mathrm{cm}^{-1}$ one, which is similar to that found in the literature for single crystal samples of comparable composition[23,55]. The HWHM width of the modes are about $50\,\mathrm{cm}^{-1}$, compared with about $25\,\mathrm{cm}^{-1}$ for the $230\,\mathrm{cm}^{-1}$ mode.

This indicates that the $x = 0.3$ and 0.35 manganite films presented in Figure 5 host COO which is static or dynamic[21,22], and that the manganite remains insulating at temperatures around 10 K. Minor spatial regions of phase-separated, conducting material cannot be ruled out from Raman measurements, however electrical transport measurements on these single-layer films confirm that they are insulating. Note, that electrical transport measurements cannot distinguish the electrical response of the manganite from the $YBa_2Cu_3O_7$, and instead a spectroscopic probe can provide crucial information. Even though, it is possible to measure the resistivity of individual layers and make an estimate of the current distribution, there can be also interactions between the layers that can modify the electrical response. This specifically relates to the explanation of the electrically conducting-to-insulating transition observed in our manganite-YBCO multilayers upon cooling below 80 K[11]. One would normally expect the resistance to fall to (near) zero at this temperature, as the YBCO transitions to a superconducting state (see e.g. Ref. 1). So, where is the current flowing in the multilayer during this measurement (when it is conducting), and in what way is the electronic state of the manganite or YBCO modified? These questions have been discussed in early publications[11,12,14,30], and our current spectroscopic study contributes further to that understanding, e.g. by giving evidence for a near-optimally doped YBCO layer and insulating manganite layer.

As the primary COO in the manganites doubles the unit cell, it is most coherent around $x = 0.5$ as there is an equal number of nominally $Mn^{3+}$ and $Mn^{4+}$ ions to form the COO state[21]. As such, we can expect the sharpest COO-derived peaks for samples with $x = 0.5$. Several peaks in the NCSMO $x = 0.5$ spectra are indeed somewhat sharper and more pronounced, such as the peaks in the $z(X'X')\bar{z}$ configuration at $340\,\mathrm{cm}^{-1}$, $520\,\mathrm{cm}^{-1}$ and $590\,\mathrm{cm}^{-1}$. More subtle, but notable, is the weaker ‘background’ intensity around $300\,\mathrm{cm}^{-1}$. When comparing peak positions of the $x = 0.5$ samples with the $x = 0.3$ and 0.35 samples, in $z(X'Y')\bar{z}$ there is an increased splitting of the two main peaks at approximately $490\,\mathrm{cm}^{-1}$, which softens $10\,\mathrm{cm}^{-1}$ compared with the $x = 0.3$ and 0.35 samples, and the $620\,\mathrm{cm}^{-1}$, which hardens $15\,\mathrm{cm}^{-1}$. There is also a $10\,\mathrm{cm}^{-1}$ softening of the 230 and $155\,\mathrm{cm}^{-1}$ peaks with respect to the $x = 0.3$ and 0.35 samples.

These observations are all consistent with an interpretation that the COO in the NCSMO $x = 0.3$ and PLCMO films is less well developed/ordered than for the NCSMO $x = 0.5$ films, or when compared with $La_{0.5}Ca_{0.5}MnO_3$ or $YMnO_3$ single crystals[23,53,55].

We note that in all films studied, both the multilayers and single manganite layer films, significant additional Raman scattering is observed around $300\,\mathrm{cm}^{-1}$. This scattering is most pronounced in samples with the manganite doped at $x = 0.3$ or 0.35, and between the temperatures 100 and 200 K in the $z(X'Y')\bar{z}$ channel. Decomposition of the spectra, such as that shown in Figure 4, requires a peak in location that is similar in intensity, if not somewhat broader, than the phonon mode at $470\,\mathrm{cm}^{-1}$ in order to fit the data. Previously, Ishii *et al.*[27] have identified magnon scattering at these energies in perovskite phase manganites.

Finally, we discuss the broad peak that is observed centered around $1000\,\mathrm{cm}^{-1}$, which splits into two distinct peaks for the $x = 0.5$ doped manganite multilayer. A similar feature has been observed before and was attributed to multi-phonon scattering[23,24]. We cannot exclude this interpretation, but note that its spectral weight does not resemble the $2\nu$-DOS spectrum. Considering the total phonon DOS measured by neutron scattering from Wdowik *et al.* for the manganites[56] and from Pintschovius *et al.* for YBCO[57], we find that the $2\nu$-DOS may add the spectral weight under $300\,\mathrm{cm}^{-1}$, but cannot explain the peak around $1000\,\mathrm{cm}^{-1}$. Even though authors in

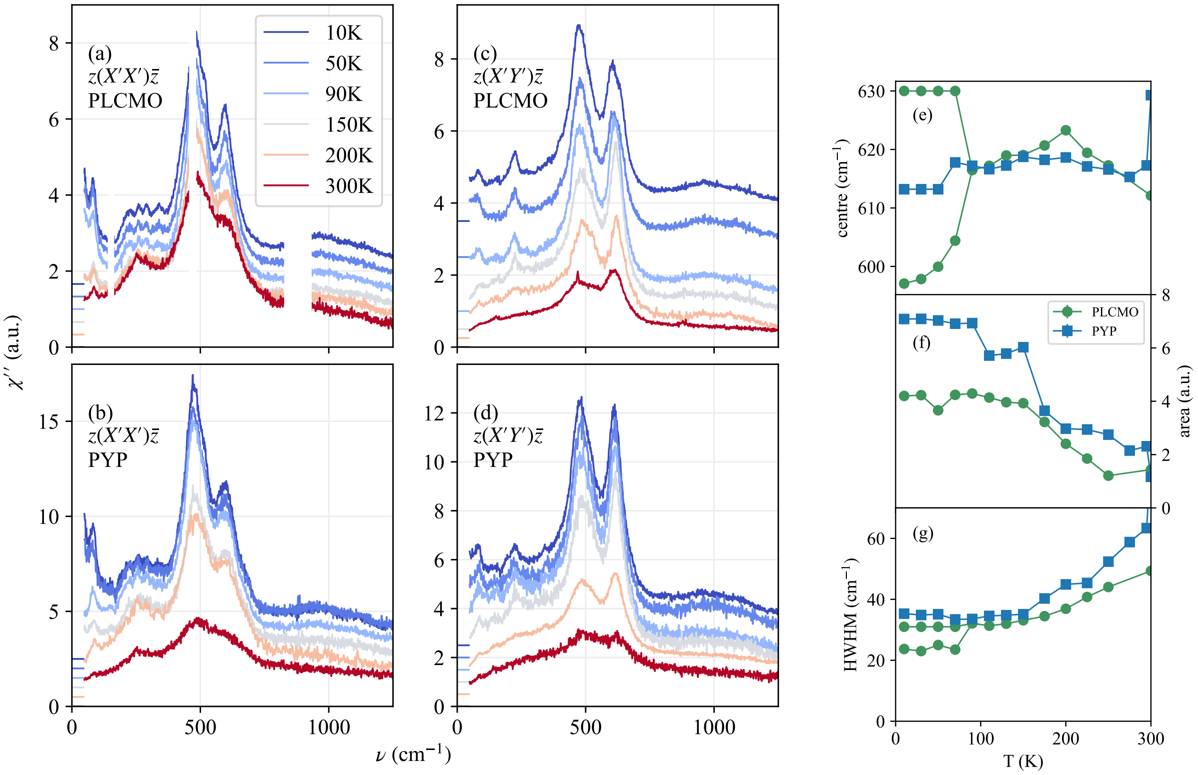

FIG. 6. Temperature dependence of the Raman response for a 20 nm thick PLCMO film and a PLCMO(20 nm) / YBCO (7 nm) / PLCMO(20 nm) multilayer (PYP). Panels (a) and (b) show the $z(X'X')\bar{z}$ scattering for PLCMO and the multilayer respectively at select temperatures. Panels (c) and (d) show the $z(X'Y')\bar{z}$ scattering. For clarity, the spectra have been vertically offset as indicated by the colour-matched zero-lines. Fitting results for (e) center frequency, (f) area and (g) half width at half maximum (HWHM) for the peak(s) around 610 cm$^{-1}$ with $z(X'Y')\bar{z}$ scattering. For the single layer PLCMO there is a resolved splitting of the mode below 90 K and a possible reduction in intensity with respect to the same mode in the multilayer sample.

Refs.[58] ascribed a similar spectral feature to two-magnon scattering in the hexagonal crystal phase manganite $YMnO_3$, we observe the 1000 cm$^{-1}$ mode well above the where a net magnetic moment can be measured in these films (at least 60 K higher)[11,12,30]. We therefore exclude that magnetic origin is a likely explanation. The development of the peak at 200 K does however suggest that it is related to the COO. This leads us to speculate that the 1000 cm$^{-1}$ arises from the photoionization of small polarons as described by Yoon *et al.*[59]. Here, a transition from a band of localized small polaron states in the paramagnetic phase into the conduction band is responsible for a broad Raman-active excitation in this energy range (120 meV). In this scenario, the polaron is localized in the COO state and suppressed by a transition from the insulating to metallic electronic transport, and the concomitant ferromagnetic transition in CMR manganites.

## D. Temperature dependence

So far we have discussed the structural and electronic characteristics of our NCSMO and PLCMO films at 10 K. In the following, we turn to the temperature dependence of PLCMO single layer films and YBCO-PLCMO multilayers.

In Figure 6 we show representative spectra from a single-layer PLCMO (20 nm) film and PLCMO(20 nm) / YBCO (7 nm) / PLCMO(20 nm) trilayer film for a range of temperatures. In these spectra, $f_{\mathrm{vac}}$ was adjusted so that the spectra have equal intensities around 1250 cm$^{-1}$. This adjustment was made to compensate changes in the focus position as the temperature was varied. For clarity, the spectra have also been vertically offset as indicated by the colour-matched zero-intensity lines. Figure 7 shows the same data but zoomed on the region around the 230 and 340 cm$^{-1}$ modes.

Here, several additional peaks are resolved below about 200 K, including the broad peak around 1000 cm$^{-1}$. Coinciding with the measurable appearance of these peaks, such as the 230 cm$^{-1}$ mode, there is also a marked increase in the area of the peaks around 470 and 610 cm$^{-1}$. This can be seen for example in the peak-fitting results shown in Figure 6 (e-g) which displays the center $\nu_0$, area $SW$ and HWHM $\gamma$ for the peak(s) around 610 cm$^{-1}$ in panels (a), (b) and (c) respectively. 200 K is significantly higher than the onset of a macroscopic magnetic moment in these films that is instead observed from below 140 K. However it does coincide with the onset of anoma-

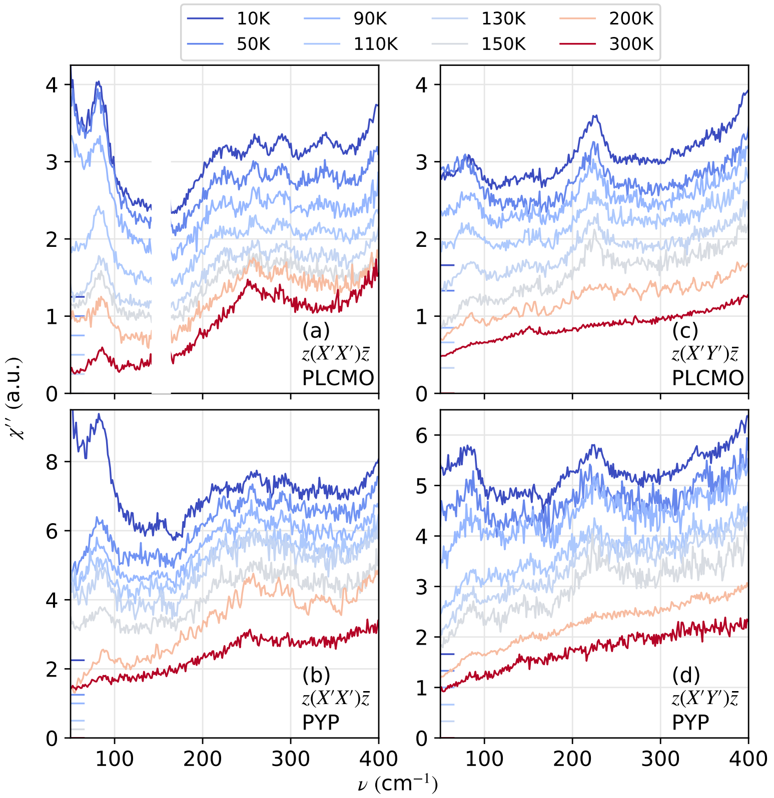

FIG. 7. Magnified view of the region around the 230 and 340 cm$^{-1}$ modes of the temperature-dependent spectra shown in Figure 6.

lous transport properties, such as spontaneous voltages and a marked non-ohmic response[14]. This implies a reduction of local symmetry and internal electric fields, which is probably due to COO, and is consistent with the appearance of additional and sharper peaks in the Raman scattering spectra. For various NCSMO manganite compositions, the temperature at which the 230 cm$^{-1}$ is resolved was seen to coincide with the development of COO as measured by Cu-L3 resonant inelastic x-ray scattering (RIXS)[12].

As the temperature is lowered further from 200 K, for most peaks there is a gradual increase in $SW$. The effect is too large to be attributable to a laser-heating effect, and as such suggests an ongoing lattice distortion further from the ideal cubic unit cell.

For the 20 nm single layer PLCMO, around 90 K there is a resolved splitting of the 610 cm$^{-1}$ mode in $z(X'Y')\bar{z}$ as seen in the top panel of Fig. 6(e). This mode is assigned as a breathing type mode involving the O of the MnO$_6$ octahedra[22,23]. The splitting is not observed for the multilayer samples or the in the 10 K data from the 100 nm thick PLCMO films. The splitting of the 610 cm$^{-1}$ mode below 90 K indicates a further reduction in symmetry of the crystal lattice that is suppressed in thicker films or by the presence of the YBCO layer.

### E. Magnetic field dependence

Figure 8(a) shows spectra for a PLCMO(10 nm) / YBCO(10 nm) superlattice in magnetic fields from 0 to 13 T. There is a non-trivial background signal due to the 30° sample tilt, which limits our ability to make a robust background subtraction to small spectral ranges and isolated peaks. Several spectral features arise from the LSAT substrate: The main substrate mode centered at 880 cm$^{-1}$ is marked with an asterisk, and the two other spectral regions in the vicinity of 470 cm$^{-1}$ and 600 cm$^{-1}$ have been masked due to a likely residual substrate contribution. In order to correct for minor drift in alignment during the measurements, we normalized the spectra so that the intensity of the 880 cm$^{-1}$ substrate peak is kept constant. We can make two main observations from the field-dependent spectral response of the multilayer. Firstly, the amplitude of the 230 cm$^{-1}$ peak is suppressed in magnetic field. This is shown in Fig. 8(b) in which a linear background has been subtracted in the narrow spectral region around the peak, and the data smoothed by adjacent averaging for visual clarity. In previous studies, we have used the area of this peak as a proxy for the charge-order parameter in the manganite[12,30]. The results of peak-fitting this region of the magnetic-field data are shown in panel (c), we have fixed the width of the 230 cm$^{-1}$ peak to be 6.5 cm$^{-1}$ and the width of the 255 cm$^{-1}$ mode to be 15 cm$^{-1}$, in order to reduce corre-

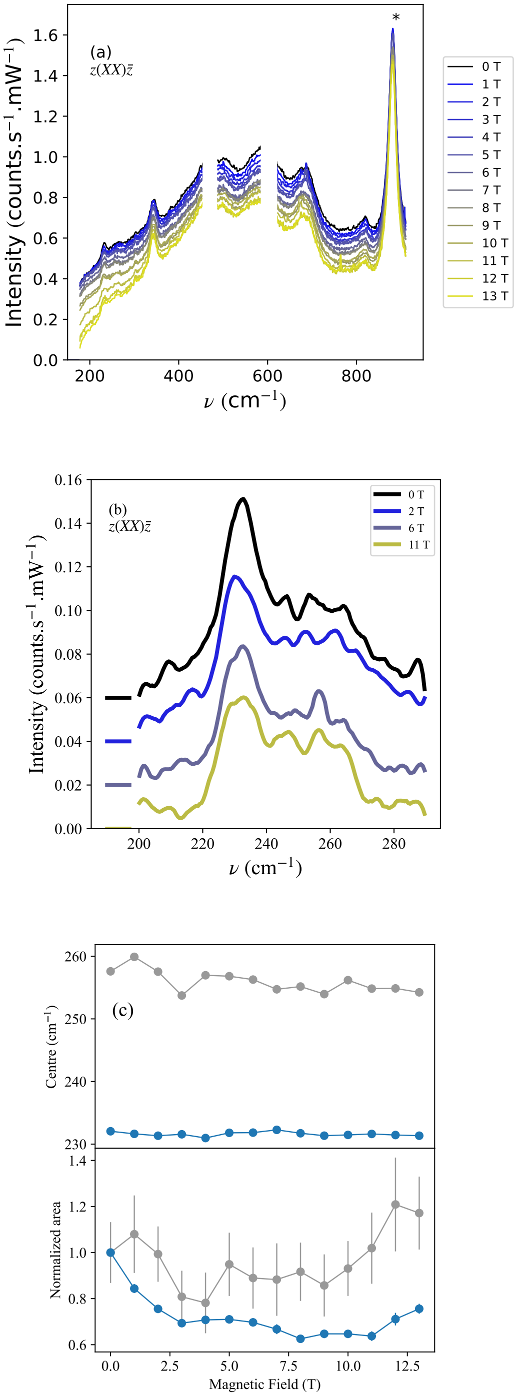

FIG. 8. (a) Magnetic field dependence of the Raman spectrum from a PLCMO(10 nm)/YBCO(10 nm) superlattice at $T = 5$ K in quasi-$z(XX)\bar{z}$ scattering geometry. The spectra have been vertically offset for clarity. The asterisk indicates an LSAT-substrate phonon. Panel (b) highlights the spectral region around the 230 cm$^{-1}$ mode that is associated with charge-order in the manganite. For visual clarity, the data in this panel are smoothed by adjacent averaging. Panel (c) shows fitting parameters of the peak area and centre positions for the two peaks highlighted in panel (b). A linear background has been subtracted in the narrow spectral region around the peak. In the fits, the widths are kept fixed at 6.5 cm$^{-1}$ and 15 cm$^{-1}$ for the 230 cm$^{-1}$ and 255 cm$^{-1}$ peaks respectively.

lations in the fits due to the peak overlapping. As the field is increased to 3 T, we observe a reduction of the 230 cm$^{-1}$ peak area by ca. 25% (blue colored fit points), which does not further change significantly with higher fields. Meanwhile, the peak area of the adjacent and less clearly defined 255 cm$^{-1}$ (grey colored fit points) peak shows no systematic variation with field. Note that even thought the error bar for the latter fit is rather big, there might be an increase of the peak area for B > 10 T.

Secondly, apart from the 230 cm$^{-1}$ mode discussed above, there is no clear field-dependence in the spectra. For example the 340 cm$^{-1}$ mode (deriving from the YBCO layers and coupled to their low-energy electronic states) and the 830 cm$^{-1}$ mode (seen only in multilayer films) show no systematic field-dependence of width or asymmetry.

The field dependent data are thus consistent with an insulating manganite layer at all fields and an incomplete suppression of charge-ordering with fields of 3 T. While this does not rule out filamentary conducting paths in the manganite, the minimal changes in the Raman spectra with field suggests that any such conducting fractions would constitute a small part of the total volume of the manganite.

## F. Interactions at Cuprate/Manganite Interface

In this section we discuss the spectral features unique to the multilayers we have studied. Fig. 9 displays the structural unit of an manganite/cuprate interface. By itself, the presence of the interface breaks the inversion symmetry presented in the site symmetry of ions in both neighboring planes as well in the unit cells adjacent to the interface. Note that in the bulk state the space groups of optimally doped YBCO – *Pmmm*[60] and e.g. LCMO - *Pnma*[61] both possess inversion symmetry. The minimal model to account for the loss of inversion at both the MnO and BaO interface planes can be presented as a transition from $D_{2h}$ to $C_{2v}$ rotation symmetry with the $C_2$ axis perpendicular to the interface at each side. Further details can be found in the Supplementary Materials. The local symmetry breaking induces additional lines in the Raman (and Infrared) spectra that arise from the phonon excitations of ions disposed at the interface.

The mutual orientation of the YBCO and manganite interfacial layers shown in Fig. 9 allows us to partly differentiate its contributions. In particular we obtain:

$$\begin{aligned} z(XX)\bar{z} =& 2[A_g + B_{1u}(z)]_{YBCO} + \\ & [3A_g + 6B_{2u}(y) + 3B_{2g} + 6A_u]_{RMnO_3} \end{aligned} \tag{4}$$

$$z(X'X')\bar{z} = 2[A_g + B_{1u}(z)]_{YBCO} + [3A_g + 6B_{2u}(y)]_{RMnO_3} \tag{5}$$

$$z(X'Y')\bar{z} = 2[340\,\mathrm{cm}^{-1}]_{YBCO} + [3B_{2g} + 6A_u]_{RMnO_3} \tag{6}$$

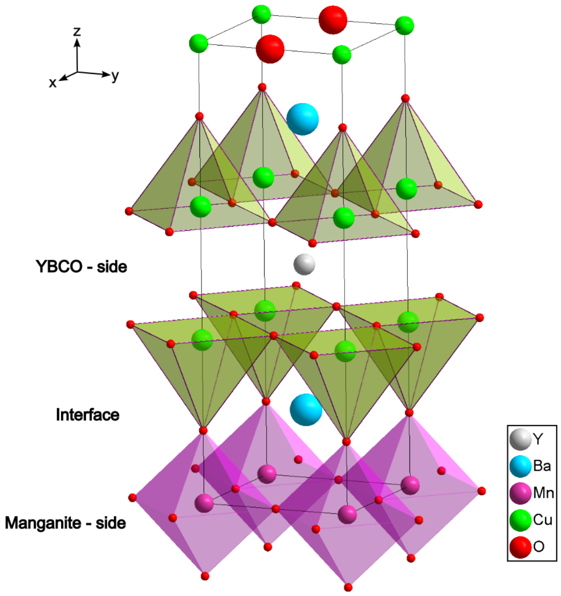

FIG. 9. The interface structural unit. The oxygen O(IV) (in YBCO notation) is a common ion connecting $CuO_5$ pyramids and $MnO_6$ octahedra.

In $z(XX)\bar{z}$ diagonal polarization, there are eight additional polar phonon modes with polarization perpendicular to the interface which are induced by the interface (denoted with a $u$). Two of them come from the YBCO side and six of them come from the manganite side. The spectra in $z(X'X')\bar{z}$ geometry contain contributions solely from the interface polar modes; these contributions are absent in the $z(X'Y')\bar{z}$ spectra and only the manganite interface modes are present. However, the line 340 $cm^{-1}$ in the $z(X'Y')\bar{z}$ geometry coming from the YBCO side (having $B_{1g}$ symmetry in the tetragonal $D_{4h}$ setting) presents oscillations of the oxygen ions from the Cu(2)O planes. Therefore the change of its properties (namely the width) compared to the bulk also indicates an involvement of the Cu(2)O plane into charge transfer mechanism although it is a secondary plane at the interface after the BaO(IV) one. In particular, this SL geometry leads to a change in the oxygen doping level of the YBCO layers at the interface by charge transfer (instead of chemical substitution), which results in a reduction of the mobile charge carrier concentration near the interface[6,62].

One of these additional Raman-active peaks is observed at 690 $cm^{-1}$, appearing in the trilayer samples as a weak shoulder to the 610 $cm^{-1}$ manganite mode, and in the superlattice samples as a pronounced peak (see Fig. 3 (a)). It is of a low symmetry appearing in all scattering channels that we measured, see Fig. 2(a), but most prominent in the parallel polarizations $z(XX)\bar{z}$ and $z(X'X')\bar{z}$. In this regard, we note that some of us have previously reported highly non-ohmic IV characteristics in these multilayers that are reminiscent of a ferroelectric moment[11], but also in single-layer films of the PLCMO manganite which do not exhibit a peak at 690 $cm^{-1}$ in their Raman spectra. There are also reported spectra showing a 690 $cm^{-1}$ mode in the response from polished single crystals of the perovskite-phase manganite $La_{0.64}Pb_{0.36}MnO_3$[59], although its origin was not discussed. These observations suggest the scenario of asymmetrically strained/distorted $MnO_6$ octahedra near the interface giving rise to a Raman-active mode at 690 $cm^{-1}$.

The superlattice samples also host an additional weak peak at 830 $cm^{-1}$ (see Fig. 2(a) and 3) that is similarly observed in all scattering channels. It has been previously seen in the Raman spectra of pure $LnMnO_3$[63] (with nominal $Mn^{3+}$ valence) and $CaMnO_3$[64] (with nominal $Mn^{4+}$ valence) and disappears under doping, which indicates that this mode is independent on the ratio of the $Mn^{3+}/Mn^{4+}$ valence state. This behaviour might be attributed to multi-phonon scattering, however, we consider this interpretation unlikely for several reasons: Firstly, the line-width is comparable to that of the single-phonon modes. Secondly, according to Ref.[56] there is not enough phonon density available at 415 $cm^{-1}$ to create a Raman peak at ca. 830 $cm^{-1}$. Note that those spectra were taken at 625 K, and with decreasing temperature the general phonon density of states will even shift to lower energy[65]. Thirdly, we observe this mode on the background of the fully suppressed 1000 $cm^{-1}$ mode; if the 830 $cm^{-1}$ mode was also originating from two-phonon scattering, it should be likewise suppressed.

We also exclude the possibility of a magnetic origin, as there appears to be no effect on this mode in a magnetic field up to 13 Tesla. To the best of our knowledge, an excitation at this energy has not been seen and associated with oxygen vacancies, neither in YBCO[66,67] nor manganite[68,69] samples. We also consider it unlikely to be a backfolded phonon mode, since its energy is higher than any phonon within the Brillouin Zone as shown by inelastic neutron scattering measurements of the total phonon DOS in manganites[56], and cuprates[57,70]. Instead, we assign the 830 $cm^{-1}$ mode as the interface-induced LO polar phonon with vibrations of the interface $MnO_6$ octahedra with the apical oxygen being O(IV) from the YBCO-BaO plane. In this scenario, the phonon is a hybridization of the above-mentioned TO polar phonons of YBCO and manganite at around 550 $cm^{-1}$ with a dynamical polar moment perpendicular to the interface. Its oscillator strength is highly enhanced by an interfacial electric dipole moment. This phonon can be seen in the case of an insulating state in the manganite layers and a granular superconductive state in the YBCO layers with presence of non-superconductive regions[11]. Otherwise, in the case of purely conductive YBCO layers its polar oscillation will be screened by the free charge carriers. Thus, the appearance of this phonon in our Raman spectra supports the scenario of the existence of non-conductive regions in the SL simultaneously in both YBCO and manganite layers. Such conductive regions being incorporated in the non-conductive (or less conductive) ones can enhance the intensity of this phonon mode, similar to what was seen in recently reported surface-enhanced Raman experiments[71].

Turning now to the lower-frequency modes highlighted in Fig. 7, which primarily originate from the manganite and are significantly modified in the multilayer samples. The modes are in general broader for the multilayers than the single layers, with a possible satellite peak next to the 230 cm$^{-1}$ mode in $z(X'Y')\bar{z}$ configuration at 195 cm$^{-1}$. These effects can also be clearly seen in the comparative spectra in Figure 3. The broadening of peaks in the multilayers appears to be temperature independent. It is unlikely to result from a decrease in crystal quality since the other phonon modes, such as those below 175 cm$^{-1}$, do not show as large an increase in width between the single-layer and SL. Although the broadening may be due to the manganite layers having dissimilar properties, we believe it is implausible in the case of the 230 cm$^{-1}$ mode in the $z(XY)\bar{z}$ channel that there is a 30 cm$^{-1}$ softening between the top and bottom PLCMO layer in the trilayer material. Hybridization with YBCO phonons, which was discussed by Driza et al.[6], may offer an explanation of these effect. Detailed lattice vibrational calculations are required to confirm this hypothesis.

Note, that yet another reason for the appearance of forbidden polar phonon modes in the Raman spectra may be due to the sample surface itself that locally breaks the inversion symmetry (see e.g. Ref.[72]). This mechanism can explain the observation of phonon modes around 740 and 830 cm$^{-1}$ in the insulating systems $LaMnO_3$[63] and $CaMnO_3$[64] that were un-assigned for a long time. Interestingly, in the Raman experiments on powder $CaMnO_3$[64] with backscattering geometry, a strong mode at 740 cm$^{-1}$ was observed, which well fits the LO polar phonon energy that has be estimated from its far-infrared data. In $La_{1-x}Sr_xMnO_3$, these Raman peaks disappear with increasing doping, since the polar phonons are screened by free charge carriers[63].

## IV. CONCLUSIONS

We report Raman spectra from thin-film multilayers of optimally doped YBCO and insulating manganites hosting COO. Our study demonstrates the suitability of using confocal Raman spectroscopy for studying such metal-oxide thin film samples down to approximately 10 nm thickness. We find that the structural quality of such films, as revealed by their phonon spectra, is comparable to that of single crystals.

All spectra exhibit significant Jahn-Teller distortions of the manganite layers that are enhanced by the degree of COO since they increase in magnitude from temperatures that are well above where a macroscopic magnetic moment is observed. These distortions indicate that those layers remain in an electrically insulating state at all temperatures below 300 K and in magnetic fields up to 13 T. The data shows that this conclusion holds in the case of cuprate-manganite multilayers, which is noteworthy because the multilayers host an unusual insulating superconducting ground state that transitions to a conducting one in a magnetic field. Electrical transport measurements of such multilayers, on the other hand, cannot distinguish the contribution of the electrical response from the individual layers.

We observe new peaks that arise at 830 cm$^{-1}$ (103 meV) and 690 cm$^{-1}$ (85.5 meV), and discuss their origin to be from the cuprate-manganite interface. In addition, there may be hybridization of some of the YBCO and manganite phonon modes, particularly around 200 cm$^{-1}$ (25 meV). This modified phonon behaviour may in turn contribute to the remarkable electronic properties of these multilayer materials.

## ACKNOWLEDGMENTS

F.L. acknowledges support from the Swiss National Science Foundation (SNSF) through an Early Postdoc.Mobility Fellowship with Project No. P2FRP2-199598. B.P.P.M. acknowledges support from the New Zealand Ministry of Business, Innovation and Employment (MBIE) through the Catalyst Seeding Fund, Contract Number CSG-VUW1901. Y.G.P. acknowledges financial support from the SNSF through the individual grants IZSEZ0_212006 and IZSEZ0_215824 of the «Scholars at Risk» Program. Work at the University of Fribourg was supported by the SNSF by the Grants No. 200020-172611 and 200021-212050.

The following abbreviations are used in this manuscript:

| | |
|---|---|
| YBCO | $YBa_2Cu_3O_{7-\delta}$ |
| high-$T_c$ SC | high-temperature superconductor |
| PLCMO | $Pr_{0.5}La_{0.2}Ca_{0.3}MnO_3$ |
| NCSMO | $Nd_{1-x}(Ca_{1-y}Sr_y)_xMnO_3$ |
| LCMO | $La_{1-x}Ca_xMnO_3$ |
| COO | charge- and orbital-order |
| *SW* | peak area underneath the Raman spectrum |
| TO | transverse optical mode |
| LO | longitudinal optical mode |

[1] J. Chakhalian, J. W. Freeland, H.-U. Habermeier, G. Cristiani, G. Khaliullin, M. van Veenendaal, and B. Keimer, “Orbital reconstruction and covalent bonding at an oxide interface,” Science **318**, 1114–1117 (2007).

[2] N. Reyren, S. Thiel, A. D. Caviglia, L. F. Kourkoutis, G. Hammerl, C. Richter, C. W. Schneider, T. Kopp, A.-S. Ruetschi, D. Jaccard, M. Gabay, D. A. Muller, J.-M. Triscone, and J. Mannhart, “Superconducting Interfaces Between Insulating Oxides,” Science **317**, 1196–1199 (2007).

[3] J. Mannhart and D. G. Schlom, “Oxide interfaces? an opportunity for electronics,” Science **327**, 1607–1611 (2010).

[4] M. Bibes, J. E. Villegas, and A. Barthélémy, “Ultrathin oxide films and interfaces for electronics and spintronics,” Advances in Physics **60**, 5–84 (2011), https://doi.org/10.1080/00018732.2010.534865.

[5] H. Y. Hwang, Y. Iwasa, M. Kawasaki, B. Keimer, N. Nagaosa, and Y. Tokura, “Emergent phenomena at oxide interfaces,” Nature materials **11**, 103 (2012).

[6] N. Driza, S. Blanco-Canosa, M. Bakr, S. Soltan, M. Khalid, L. Mustafa, K. Kawashima, G. Christiani, H.-U. Habermeier, G. Khaliullin, C. Ulrich, M. Le Tacon, and B. Keimer, “Long-range transfer of electron-phonon coupling in oxide superlattices,” Nature Materials **11** (2012), 10.1038/nmat3378.

[7] K. Rogdakis, J. Seo, Z. Viskadourakis, Y. Wang, L. A. Qune, E. Choi, J. Burton, E. Tsymbal, J. Lee, and C. Panagopoulos, “Tunable ferroelectricity in artificial tri-layer superlattices comprised of non-ferroic components,” Nature communications **3**, 1064 (2012).

[8] J. Chakhalian, J. W. Freeland, A. J. Millis, C. Panagopoulos, and J. M. Rondinelli, “Emergent properties in plane view: Strong correlations at oxide interfaces,” Rev. Mod. Phys. **86**, 1189–1202 (2014).

[9] M. Lorenz, M. R. Rao, T. Venkatesan, E. Fortunato, P. Barquinha, R. Branquinho, D. Salgueiro, R. Martins, E. Carlos, A. Liu, *et al.*, "The 2016 oxide electronic materials and oxide interfaces roadmap," Journal of Physics D: Applied Physics **49**, 433001 (2016).

[10] J. P. Bange, V. Roddatis, L. Schüler, F. Lyzwa, M. Keunecke, S. Lopatin, V. Bruchmann-Bamberg, and V. Moshnyaga, "Charge transfer control of emergent magnetism at srmno3/lamno3 interfaces," Advanced Materials Interfaces **9**, 2201282 (2022), https://onlinelibrary.wiley.com/doi/pdf/10.1002/admi.202201282.

[11] B. P. P. Mallett, J. Khmaladze, P. Marsik, E. Perret, A. Cerreta, M. Orlita, N. Biškup, M. Varela, and C. Bernhard, "Granular superconductivity and magnetic-field-driven recovery of macroscopic coherence in a cuprate/manganite multilayer," Phys. Rev. B **94**, 180503(R) (2016).

[12] E. Perret, C. Monney, S. Johnston, J. Khmaladze, F. Lyzwa, R. Gaina, M. Dantz, J. Pelliciari, C. Piamonteze, B. Mallett, M. Minola, B. Keimer, T. Schmitt, and C. Bernhard, "Coupled cu and mn charge and orbital orders in $\mathrm{YBa_2Cu_3O_7/Nd\ _{0.65}(Ca\ _{1-y}Sr_y)_{0.35}MnO_3}$ multilayers," Communications Physics **1**, 45 (2018).

[13] N. Bonmassar, G. Christiani, T. Heil, G. Logvenov, Y. E. Suyolcu, and P. A. van Aken, "Superconductivity at interfaces in cuprate-manganite superlattices," Advanced Science **10**, 2301495 (2023), https://onlinelibrary.wiley.com/doi/pdf/10.1002/advs.202301495.

[14] R. Gaina, S. Sarkar, M. Soulier, J. Khmaladze, E. Perret, A. Tcakaev, V. Hinkov, M. Bonura, E. Weschke, and C. Bernhard, "Magnetic field dependence of the copper charge density wave order in a $\mathrm{yba_2cu_3o_7/nd_{0.65}(Ca_{0.7}Sr_{0.3})_{0.35}mno_3}$ superlattice," Phys. Rev. B **104**, 174513 (2021).

[15] B. Stoddart-Stones, X. Montiel, M. G. Blamire, and J. W. A. Robinson, "Competition between the superconducting spin-valve effect and quasiparticle spin-decay in superconducting spin-valves," Communications Physics **5** (2022), 10.1038/s42005-022-01003-0.

[16] R. de Andrés Prada, T. Golod, O. M. Kapran, E. A. Borodianskyi, C. Bernhard, and V. M. Krasnov, "Memory-functionality superconductor/ferromagnet/superconductor junctions based on the high-$T_c$ cuprate superconductors $\mathrm{yba_2cu_3o_{7-x}}$ and the colossal magnetoresistive manganite ferromagnets $\mathrm{la_{2/3}}X_{1/3}\mathrm{mno_{3+\delta}}(x = \mathrm{Ca,\ Sr})$," Phys. Rev. B **99**, 214510 (2019).

[17] M. F. Limonov, A. I. Rykov, S. Tajima, and A. Yamanaka, "Superconductivity-induced effects on phononic and electronic raman scattering in twin-free $\mathrm{yba_2cu_3o_{7-x}}$ single crystals," Phys. Rev. B **61**, 12412–12419 (2000).

[18] M. Opel, R. Nemetschek, C. Hoffmann, R. Philipp, P. Müller, R. Hackl, I. Tüttő, A. Erb, B. Revaz, E. Walker, *et al.*, "Carrier relaxation, pseudogap, and superconducting gap in high-$T_c$ cuprates: A Raman scattering study," Physical Review B **61**, 9752 (2000).

[19] R. Brahem, Z. Raddaoui, and M. Bourguiba, "Effect of a-site rare earth substitution on structural, colossal permittivity, and impedance properties of la0.67r0.03ca0.2sr0.1mno3 (r=pr, er) manganite," Journal of Materials Science: Materials in Electronics **33** (2022), 10.1007/s10854-021-07611-w.

[20] M. Bakr, S. M. Souliou, S. Blanco-Canosa, I. Zegkinoglou, H. Gretarsson, J. Strempfer, T. Loew, C. T. Lin, R. Liang, D. A. Bonn, W. N. Hardy, B. Keimer, and M. Le Tacon, "Lattice dynamical signature of charge density wave formation in underdoped $\mathrm{yba_2cu_3o_{6+x}}$," Phys. Rev. B **88**, 214517 (2013).

[21] Y. Tomioka, Y. Okimoto, J. H. Jung, R. Kumai, and Y. Tokura, "Critical control of competition between metallic ferromagnetism and charge/orbital correlation in single crystals of perovskite manganites," Phys. Rev. B **68**, 094417 (2003).

[22] K. Yamamoto, T. Kimura, T. Ishikawa, T. Katsufuji, and Y. Tokura, "Raman spectroscopy of the charge-orbital ordering in layered manganites," Phys. Rev. B **61**, 14706–14715 (2000).

[23] M. V. Abrashev, J. Bäckström, L. Börjesson, M. Pissas, N. Kolev, and M. N. Iliev, "Raman spectroscopy of the charge- and orbital-ordered state in $\mathrm{la_{0.5}ca_{0.5}mno_3}$," Phys. Rev. B **64**, 144429 (2001).

[24] M. N. Iliev, M. V. Abrashev, V. N. Popov, and V. G. Hadjiev, "Role of jahn-teller disorder in raman scattering of mixed-valence manganites," Phys. Rev. B **67**, 212301 (2003).

[25] M. Cardona, "Raman scattering in high-$t_c$ superconductors: phonons, electrons, and electron-phonon interaction," Physica C: Superconductivity **317**, 30–54 (1999).

[26] S. Sugai and T. Hosokawa, "Relation between the superconducting gap energy and the two-magnon Raman peak energy in $\mathrm{Bi\ _2Sr_2Ca_{1-x}Y_xCu_2O_{8+\delta}}$," Physical Review Letters **85**, 1112–1115 (2000).

[27] I. Ishii, Y. Tokunaga, J. Fujioka, Y. Onose, and Y. Tokura, "Optical characterization of spin-charge-orbital orders in $\mathrm{Pr(Sr_{1-y}Ca_y)_2mn_2o_7}$," Phys. Rev. B **82**, 245103 (2010).

[28] D. Kiphart, Y. Harkavyi, K. Balin, J. Szade, B. Mróz, P. Kuświk, S. Jurga, and M. Wiesner, "Investigations of proximity-induced superconductivity in the topological insulator $\mathrm{bi_2te_3}$ by microraman spectroscopy," Scientific Reports **11** (2021), 10.1038/s41598-021-02475-w.

[29] M. Hepting, M. Minola, A. Frano, G. Cristiani, G. Logvenov, E. Schierle, M. Wu, M. Bluschke, E. Weschke, H.-U. Habermeier, E. Benckiser, M. Le Tacon, and B. Keimer, "Tunable charge and spin order in $\mathrm{prnio_3}$ thin films and superlattices," Phys. Rev. Lett. **113**, 227206 (2014).

[30] J. Khmaladze, S. Sarkar, M. Soulier, F. Lyzwa, R. de Andres Prada, E. Perret, B. P. P. Mallett, M. Minola, B. Keimer, and C. Bernhard, "Granular superconductivity and charge/orbital order in $\mathrm{yba_2cu_3o_7}$/manganite trilayers," Phys. Rev. Materials **3**, 084801 (2019).

[31] Y.-J. Kim, H.-S. Park, and C.-H. Yang, "Raman imaging of ferroelastically configurable jahn-teller domains in lamno3," npj Quantum Materials **6**, 62 (2021).

[32] V. K. Malik, I. Marozau, S. Das, B. Doggett, D. K. Satapathy, M. A. Uribe-Laverde, N. Biskup, M. Varela, C. W. Schneider, C. Marcelot, J. Stahn, and C. Bernhard, "Pulsed laser deposition growth of heteroepitaxial $\mathrm{YBa_2Cu_3O_7/La_{0.67}Ca_{0.33}MnO_3}$ superlattices on $\mathrm{NdGaO_3}$ and $\mathrm{Sr_{0.7}La_{0.3}Al_{0.65}Ta_{0.35}O_3}$ substrates," Phys. Rev. B **85**, 054514 (2012).

[33] F. Lyzwa, "Phononic and electronic excitations in complex oxides studied with advanced infrared and raman spectroscopy techniques," PhD Thesis (2021), 10.51363/unifr.sth.2022.002.

[34] M. Hepting, D. Kukuruznyak, E. Benckiser, M. L. Tacon, and B. Keimer, "Raman light scattering on ultra-thin films of $\mathrm{LaNiO_3}$ under compressive strain," Physica B: Condensed Matter **460**, 196 – 198 (2015), special Issue on Electronic Crystals (ECRYS-2014).

[35] G. E. Jellison, D. H. Lowndes, and R. F. Wood, "Importance of temperature-dependent optical properties for raman-temperature measurements for silicon," Phys. Rev. B **28**, 3272–3276 (1983).

[36] P. Lemmens, K. Y. Choi, V. Gnezdilov, E. Y. Sherman, D. P. Chen, C. T. Lin, F. C. Chou, and B. Keimer, "Anomalous electronic raman scattering in $\mathrm{na}_x\mathrm{coo_2} \cdot y\mathrm{h_2O}$," Phys. Rev. Lett. **96**, 167204 (2006).

[37] P. Thompson, D. E. Cox, and J. B. Hastings, "Rietveld refinement of Debye–Scherrer synchrotron X-ray data from $\mathrm{Al\ _2\ O\ _3}$," Journal of Applied Crystallography **20**, 79–83 (1987).

[38] Y. Liu, S. Niu, T. Orvis, H. Zhang, H. Zhao, H. Wang, and J. Ravichandran, "Epitaxial growth and electrical properties of vo2 on [laalo3]0.3[sr2altao6]0.7 (111) substrate," Journal of Vacuum Science & Technology A **36**, 061506 (2018).

[39] L. Gasparov, T. Jegorel, L. Loetgering, S. Middey, and J. Chakhalian, "Thin film substrates from the raman spectroscopy point of view," Journal of Raman Spectroscopy **45**, 465–469 (2014).

[40] F. Lyzwa, A. Chan, J. Khmaladze, K. Fürsich, B. Keimer, C. Bernhard, M. Minola, and B. P. P. Mallett, "Backfolded acoustic phonons as ultrasonic probes in metal-oxide superlattices," Phys. Rev. Materials **4**, 043606 (2020).

[41] G. Blumberg, P. Abbamonte, M. V. Klein, W. C. Lee, D. M. Ginsberg, L. L. Miller, and A. Zibold, "Resonant two-magnon Raman scattering in cuprate antiferromagnetic insulators," Phys. Rev. B **53**, R11930–R11933 (1996).

[42] I. Duričković, R. Claverie, P. Bourson, M. Marchetti, J.-M. Chassot, and M. D. Fontana, "Water–ice phase transition probed by raman spectroscopy," Journal of Raman Spectroscopy **42**, 1408–1412 (2011).

[43] L. A. Farrow, T. Venkatesan, W. A. Bonner, X. D. Wu, A. Inam, and M. S. Hegde, "Raman scattering investigation of a single-crystal-like $\mathrm{YBa_2Cu_3O_{7\text{-}y}}$ film," Journal of Applied Physics **65**, 4452–4453 (1989), https://pubs.aip.org/aip/jap/article-pdf/65/11/4452/8003932/4452_1_online.pdf.

[44] M. Bakr, A. P. Schnyder, L. Klam, D. Manske, C. T. Lin, B. Keimer, M. Cardona, and C. Ulrich, "Electronic and phononic raman scattering in detwinned $\mathrm{yba_2cu_3o_{6.95}}$ and $\mathrm{y_{0.85}ca_{0.15}ba_2cu_3o_{6.95}}$: $s$-wave admixture to the $d_{x^2-y^2}$-wave order parameter," Phys. Rev. B **80**, 064505 (2009).

[45] The $\mathrm{La_{0.5}Ca_{0.5}MnO_3}$ spectra from Abrashev *et al.* are qualitatively sim-

ilar to the spectra of Dediu *et al.* obtained from $Pr_{0.65}Ca_{0.35}MnO_3$ samples that were polycrystalline[73], and therefore represent an average over all polarization configurations. We note that the spectra for $La_{0.7}Ca_{0.3}MnO_3$ are somewhat different, primarily with the modes around $500\,cm^{-1}$ much weaker[6,74].

[46] B. Friedl, C. Thomsen, H.-U. Habermeier, and M. Cardona, "Intensity anomalies of raman-active phonons in the superconducting state of $YBa_2Cu_3O_{7-\delta}$ ," Solid state communications **78**, 291–294 (1991).

[47] O. V. Misochko, K. Kisoda, K. Sakai, and S. Nakashima, "Dynamics of low-frequency phonons in the $yba_2cu_3o_{7-x}$ superconductor studied by time- and frequency-domain spectroscopies," Phys. Rev. B **61**, 4305–4313 (2000).

[48] E. Baldini, A. Mann, B. P. P. Mallett, C. Arrell, F. van Mourik, T. Wolf, D. Mihailovic, J. L. Tallon, C. Bernhard, J. Lorenzana, and F. Carbone, "Clocking the onset of bilayer coherence in a high-$T_c$ cuprate," Phys. Rev. B **95**, 024501 (2017).

[49] A. M. Glazer, "The classification of tilted octahedra in perovskites," Acta Cryst. **B28**, 3384 (1972).

[50] C. J. Howard and H. T. Stokes, "Group-theoretical analysis of octahedral tilting in perovskites," Acta. Cryst. **B58**, 782 (1998).

[51] Note that epitaxial growth on a cubic substrate forces a tetragonal unit-cell to be adopted by the manganite for the first few nanometers from the substrate. The in-plane unit cell axes, which we label as the *a* and *b* axes, are about 2 % larger than the out-of-plane axis, that we label the '*c*' axis. Here, we only probe in-plane Raman response, which in the customary notation for single crystal manganites would be the *ac*-plane as the doubled unit cell, the *b*-direction customarily, should be in the out-of-plane direction.

[52] Y. Tokura, "Critical features of colossal magnetoresistive manganites," Reports on Progress in Physics **69**, 797 (2006).

[53] M. N. Iliev, M. V. Abrashev, H.-G. Lee, V. N. Popov, Y. Y. Sun, C. Thomsen, R. L. Meng, and C. W. Chu, "Raman spectroscopy of orthorhombic perovskite-like $ymno_3$ and $lamno_3$," Phys. Rev. B **57**, 2872–2877 (1998).

[54] E. Granado, N. O. Moreno, A. García, J. A. Sanjurjo, C. Rettori, I. Torriani, S. B. Oseroff, J. J. Neumeier, K. J. McClellan, S.-W. Cheong, and Y. Tokura, "Phonon raman scattering in $R_{1-x}A_x mno_{3+\delta}(r = \mathrm{La}, \mathrm{Pr}; a = \mathrm{Ca}, \mathrm{Sr})$," Phys. Rev. B **58**, 11435–11440 (1998).

[55] L. Martın-Carrón and A. De Andrés, "Raman phonons and the Jahn-Teller transition in $RMnO_3$ manganites," Journal of alloys and compounds **323**, 417–421 (2001).

[56] U. D. Wdowik, M. M. Koza, and T. Chatterji, "Phonons in lanthanum manganite: Inelastic neutron scattering and density functional theory studies," Phys. Rev. B **86**, 174305 (2012).

[57] L. Pintschovius and W. Reichardt, *Phonon Dispersions and Phonon Density-of-States in Copper-Oxide Superconductors*, edited by A. Furrer, Neutron Scattering in Layered Copper-Oxide Superconductors (Springer, Dordrecht, 1998).

[58] J.-i. Takahashi, K. Hagita, K. Kohn, Y. Tanabe, and E. Hanamura, "Anomalously broad raman scattering spectrum due to two-magnon excitation in hexagonal $ymno_3$," Phys. Rev. Lett. **89**, 076404 (2002).

[59] S. Yoon, H. L. Liu, G. Schollerer, S. L. Cooper, P. D. Han, D. A. Payne, S.-W. Cheong, and Z. Fisk, "Raman and optical spectroscopic studies of small-to-large polaron crossover in the perovskite manganese oxides," Phys. Rev. B **58**, 2795–2801 (1998).

[60] A. Williams, G. H. Kwei, R. B. Von Dreele, I. D. Raistrick, and D. L. Bish, "Joint x-ray and neutron refinement of the structure of superconducting $yba_2cu_3o_{7-x}$: Precision structure, anisotropic thermal parameters, strain, and cation disorder," Phys. Rev. B **37**, 7960–7962 (1988).

[61] F. Millange, V. Caignaert, G. Mather, E. Suard, and B. Raveau, "Low temperature orthorhombic to monoclinic transition due to size effect in $Nd_{0.7}Ca_{0.3}$-$SrMnO_3$: Evidence for a new type of charge ordering," Journal of Solid State Chemistry **127**, 131–135 (1996).

[62] A. Seo, A. V. Boris, G. Cristiani, H.-U. Habermeier, and B. Keimer, "Optical characteristics of charge carrier transfer across interfaces between $YBa_2Cu_3o_{6+\delta}$ and $La_{0.7}Ca_{0.3}Mno_3$," Phys. Rev. B **99**, 064501 (2019).

[63] K.-Y. Choi, P. Lemmens, G. Güntherodt, Y. G. Pashkevich, V. P. Gnezdilov, P. Reutler, L. Pinsard-Gaudart, B. Büchner, and A. Revcolevschi, "Orbiton-mediated multiphonon scattering in $la_{1-x}sr_xMno_3$," Phys. Rev. B **72**, 024301 (2005).

[64] V. Goian, S. Kamba, F. Borodavka, D. Nuzhnyy, M. Savinov, and A. A. Belik, "The manifestation of spin-phonon coupling in CaMnO3," Journal of Applied Physics **117**, 164103 (2015), https://pubs.aip.org/aip/jap/article-pdf/doi/10.1063/1.4918659/14862344/164103_1_online.pdf.

[65] K.-Y. Choi, P. Lemmens, T. Sahaoui, G. Güntherodt, Y. G. Pashkevich, V. P. Gnezdilov, P. Reutler, L. Pinsard-Gaudart, B. Büchner, and A. Revcolevschi, "Existence of orbital polarons in ferromagnetic insulating $la_{1-x}sr_xMno_3$ $(0.11 \leqslant x \leqslant 0.14)$ revealed by giant phonon softening," Phys. Rev. B **71**, 174402 (2005).

[66] C. Camerlingo, I. Delfino, and M. Lepore, "Micro-raman spectroscopy on ybco films during heat treatment," Superconductor Science and Technology **15**, 1606 (2002).

[67] B. H. Moeckly, R. A. Buhrman, and P. E. Sulewski, "Micro-raman spectroscopy of electromigration-induced oxygen vacancy aggregation in $YBa_2Cu_3O_{7-\delta}$," Applied Physics Letters **64**, 1427–1429 (1994).

[68] S. Merten, O. Shapoval, B. Damaschke, K. Samwer, and V. Moshnyaga, "Magnetic-field-induced suppression of jahn-teller phonon bands in $(la_0.6pr_0.4)_0.7ca_0.3mno_3$: the mechanism of colossal magnetoresistance shown by raman spectroscopy," Scientific Reports **9**, 2387 (2019).

[69] C. Xiang-Bai, M. Thi, I. Yang, D. Lee, and T. Noh, "A raman study of the origin of oxygen defects in hexagonal manganite thin films," Chinese Physics Letters **29**, 126103 (2012).

[70] B. Renker, F. Gompf, E. Gering, D. Ewert, H. Rietschel, and A. Dianoux, "Strong changes in the phonon spectra of 123 superconductors by varying oxygen concentration," Zeitschrift für Physik B Condensed Matter **73** (1988), 10.1007/BF01314268.

[71] S. Merten, V. Bruchmann-Bamberg, B. Damaschke, K. Samwer, and V. Moshnyaga, "Jahn-teller reconstructed surface of the doped manganites shown by means of surface-enhanced raman spectroscopy," Phys. Rev. Materials **3**, 060401 (2019).

[72] V. Gnezdilov, Y. G. Pashkevich, H. Berger, E. Pomjakushina, K. Conder, and P. Lemmens, "Helical fluctuations in the raman response of the topological insulator $bi_2se_3$," Phys. Rev. B **84**, 195118 (2011).

[73] V. Dediu, C. Ferdeghini, F. C. Matacotta, P. Nozar, and G. Ruani, "Jahn-teller dynamics in charge-ordered manganites from raman spectroscopy," Phys. Rev. Lett. **84**, 4489–4492 (2000).

[74] V. Podobedov, D. Romero, A. Weber, J. P. Rice, R. Schreekala, M. Rajeswari, R. Ramesh, T. Venkatesan, and H. Drew, "Diagnostics of "colossal" magnetoresistance manganite films by Raman spectroscopy," Applied physics letters **73**, 3217–3219 (1998).